Dissociation Kinetics of Energy-Selected $(C_6H_6)_2Cr^+$ Ions: Benzene−Chromium Neutral and Ionic Bond Energies†

Yue Li and Tomas Baer*

Department of Chemistry, University of North Carolina, Chapel Hill, North Carolina 27599-3290

Received: February 6, 2002; In Final Form: April 29, 2002

Threshold photoelectron−photoion coincidence spectroscopy has been used to investigate the dissociation kinetics of the bis(benzene) chromium ion, $(C_6H_6)_2Cr^+$. The dissociation of the $(C_6H_6)_2Cr^+$ ion proceeds by the sequential loss of the two benzene ligands. The two benzene-loss reactions were found to be metastable (lifetimes in the microsecond range) at photon energies close to the dissociation limits of the precursor ions. By simulating the resulting asymmetric time-of-flight peak shapes and breakdown diagram, the 0 K appearance energies of the product ions $C_6H_6Cr^+$ and Cr^+ were determined to be 7.91 ± 0.15 and 9.61 ± 0.18 eV, respectively. The two C_6H_6−Cr bond energies in the $(C_6H_6)_2Cr^+$ ion were determined to be 2.51 ± 0.15 and 1.70 ± 0.15 eV, respectively. Using the heats of formation of the fully dissociated products, C_6H_6 and Cr^+, the 298 K heats of formation of $(C_6H_6)_2Cr$, $(C_6H_6)_2Cr^+$, and $C_6H_6Cr^+$ were obtained to be 286 ± 17, 804 ± 18, and 968 ± 15 kJ/mol, respectively. Neutral C_6H_6−Cr bond energies of 2.78 and 0.06 eV were determined for the first and second losses of the benzene ligand, respectively.

Introduction

The electronic structures and reactivity features of sandwich molecules have attracted the attention of theoreticians and experimentalists for several decades.[1,2] Bis(benzene) chromium is the best-known group VIB sandwich molecule, which is formally an 18-electron coordinately saturated complex with a ground-state configuration of $(e_{2g})^4(a_{1g})^2$ $(^1A_{1g})$.[1,3] This molecule has been shown to have D_{6h} symmetry by X-ray crystallography,[4,5] electron diffraction,[6] and theoretical calculations.[7−11] The photoelectron spectra (PES) of $(C_6H_6)_2Cr$ have been measured by several groups.[12−15] Several vertical ionization energy (IE) results have been reported, including 5.4,[1,3,12,13] 5.45,[15] 5.7,[16] and 5.473 eV.[14] The electron-transfer equilibrium measurement yielded an adiabatic IE value of 5.45 eV.[14]

In the studies of the ionization and dissociation dynamics of $(C_6H_6)_2Cr$ using laser photoionization[17,18] or electron ionization (EI),[19−21] this molecule (or its ion) was found to dissociate by successive loss of the benzene ligands. The electron ionization studies[19−21] also reported the appearance energies (AE) of the fragment ions $C_6H_6Cr^+$ and Cr^+. Using these AE values, the bond energies and thermochemical results can be determined. However, the results obtained by electron ionization studies are often inaccurate because ions are not energy-selected in these experiments, and the sample's thermal energy distribution and kinetic shift are neglected in the data analysis.

The most accurate study of the ionic bond energies of this molecule was reported by Meyer et al.,[22] who studied the collision-induced dissociation (CID) of the $(C_6H_6)_2Cr^+$ and $C_6H_6Cr^+$ ions in a guided ion beam mass spectrometer. They obtained $C_6H_6Cr^+$−C_6H_6 and C_6H_6−Cr^+ bond energies of 2.40 and 1.76 eV, respectively. Because of the large number of vibrational modes and the relatively large bond energies, the rate constants at the dissociation threshold are expected to be very slow. As a result, it was essential to model the dissociation reaction with RRKM theory using assumed transition-state parameters. From a comparison with the theoretical bond energies, they concluded that a loose transition-state structure is more appropriate.

Because of the difficulties associated with bond energy determinations, we undertook this study to provide $(C_6H_6)_2Cr^+$ bond energy data from a second experimental method. In addition, our recent investigation of a related molecular system, benzene chromium tricarbonyl, $C_6H_6Cr(CO)_3$,[23] provided bond energies and heats of formation of all of the neutral and ionic dissociation products. This companion study of $(C_6H_6)_2Cr$ involves a similar intermediate structure of C_6H_6Cr, whose energy can be related to the results for $C_6H_6Cr(CO)_3$. We report here on the gas-phase dissociation kinetics of energy-selected $(C_6H_6)_2Cr^+$ ions using threshold photoelectron−photoion coincidence (TPEPICO) spectroscopy. The results obtained by TPEPICO are similar to those obtained by the previously mentioned collision-induced dissociation study[22] in that both experiments require RRKM theory treatment of the data. An important difference is that we directly measure the dissociation rate constants by analyzing the experimental product-ion time-of-flight distributions and, thus, obtain experimental transition-state parameters. The transition-state parameter is an important diagnostic for assessing the validity of assigning the dissociation limit with the bond energy. This assignment is only valid if there is no reverse activation energy. The absence of a reverse activation barrier is associated with a loose transition state, whereas a barrier is associated with a tight transition state. A second difference is that, because we measure the appearance energy of the products, we obtain the energy difference between the neutral starting compound and the final ionic products and can thus relate the ion energetics to the neutral thermochemistry. Finally, the time scales of the two experiments are different. Ions in the CID experiment are required to react within 100 μs, whereas ions in our TPEPICO study are collected within 20 μs.

† Part of the special issue "Jack Beauchamp Festschrift".
* To whom correspondence should be addressed.

10.1021/jp020341u CCC: $22.00
Published on Web 08/27/2002

Experimental Approach

The threshold photoelectron−photoion coincidence apparatus has been described in detail previously.[24] Briefly, sample vapor was leaked into the experimental chamber through a 1.0-mm-diameter inlet (2.5 cm long) and then ionized with vacuum ultraviolet (VUV) light from an H_2 discharge lamp dispersed by a 1-m normal-incidence monochromator. The VUV wavelengths were calibrated using the hydrogen Lyman-α line. The ions and the electrons were extracted in opposite directions with an electric field of 20 V/cm. Threshold photoelectrons were selected by a steradiancy analyzer that consists of a flight tube with small apertures that stop energetic electrons with perpendicular velocity components. Further discrimination against the energetic electrons was provided by a hemispherical electrostatic sector analyzer resulting in a 35-meV combined photon and electron energy resolution. The ions were accelerated to 100 eV in the first 5-cm-long acceleration region and then were accelerated to 220 eV in a short second region. The ions were detected with a multichannel plate detector after drifting through a 30-cm field-free drift region, and the electrons were detected with a channeltron electron multiplier. The electron and ion signals served as start and stop pulses for measuring the ion time-of-flight (TOF), and the TOF for each coincidence event was stored in a multichannel pulse height analyzer. TOF distributions were obtained in 1−72 h depending on the photon intensity and the desired spectrum quality.

The TPEPICO spectra were used for two purposes. First, the fractional abundances of the precursor and the product ions were measured as a function of the photon energy (breakdown diagram). Second, the product-ion TOF distributions were measured at energies close to the dissociation limits. Slowly dissociating (metastable) ions decay in the first acceleration region, and the resulting product-ion TOF distribution is asymmetrically broadened toward long TOF. The asymmetric peak shapes can be analyzed to extract the ion dissociation rate constants as a function of the ion internal energy. These two types of information were used together in the data analysis.

The bis(benzene) chromium sample [$(C_6H_6)_2Cr$, 97%, Strem Chemicals] was used without further purification.

Determination of the Sample Temperature. The data analysis requires a knowledge of the sample temperature because simulation of the data involves averaging over the internal energy distribution. Because of its low vapor pressure, it was necessary to heat the $(C_6H_6)_2Cr$ sample to obtain sufficient signal. Although the thermocouple attached to the sample cell read 130 °C, the real sample temperature was only 67 °C. The real sample temperature was determined by calibrating the inlet temperature with the $C_5H_5Mn(CO)_3$ molecule, whose TPEPICO spectrum could be measured at both room and elevated temperatures. The lower-than-measured temperature is a result of sample cooling as it passed through a 2.5-cm-long quartz tube. No $C_6H_6^+$ ions were observed in the mass spectra, which indicates that thermal decomposition of the sample did not occur at the experimental temperature.

Quantum Chemical Calculations. Vibrational frequencies and rotational constants of the equilibrium structures and transition states are required for the simulations and analysis of the experimental data. The frequencies of neutral $(C_6H_6)_2Cr$ were obtained by quantum chemical calculations in this study. The $(C_6H_6)_2Cr$ structure was fully optimized at the Hartree−Fock (HF) level; the 6-31G(d) basis set was used for the carbon and hydrogen atoms, whereas the LANL2DZ[25] basis set was used for the chromium atom. All efforts to calculate the structure and vibrational frequencies of the $(C_6H_6)_2Cr^+$ ion failed even after 2000 h of Origin-2000 time. As a result, the estimated vibrational frequencies of ionic $(C_6H_6)_2Cr^+$, taken from Meyer et al.,[22] are based on the frequencies of neutral $(C_6H_6)_2Cr$ and the iodo salt, $[(C_6H_6)_2Cr]I$. The frequencies of $C_6H_6Cr^+$ are taken from a previous DFT calculation.[23] The ground state of the Cr atom is $3d^54s^1(^7S_3)$. In the ground state, the $(C_6H_6)_2Cr$ molecule is a singlet ($^1A_{1g}$),[1] and $(C_6H_6)_2Cr^+$ is $^2A_1$,[14] whereas the $C_6H_6Cr^+$ ion is $^6A_1$.[22, 23, 26]

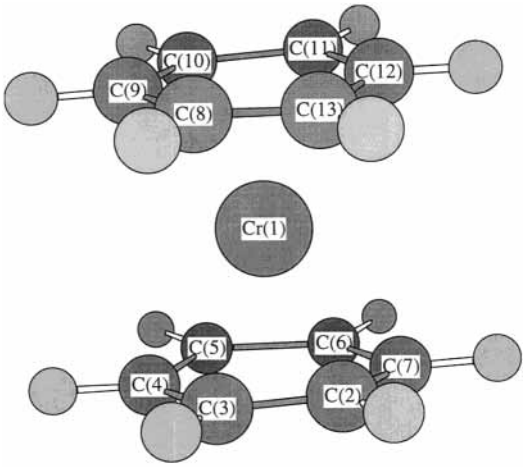

Figure 1. Equilibrium structure and main geometrical parameters of neutral $(C_6H_6)_2Cr$.

Figure 1 shows the structure and main parameters of neutral $(C_6H_6)_2Cr$ obtained at the HF level. Two benzene rings are nearly parallel to each other and of the equal distances from the chromium atom; thus, the molecule has nearly D_{6h} symmetry. The C−Cr distances are about 2.20 Å, comparable to the electron diffraction result[6] and several other theoretical results.[10,11]

To relate the dissociation energy to a bond energy, it must be established that the reaction has no reverse barrier. Although we were not successful in testing this via our calculations, we can establish it on the basis of the experimental fit of the RRKM theory to the rate data. If the transition state is loose (i.e., no reverse barrier), the determination of the transition-state structures and frequencies should be based on variational transition state theory (VTST).[27−29] Because the transition states are expected to lie close to the dissociation limits, we used RRKM theory with the precursor-ion frequencies as the estimates for the transition-state frequencies. In the simulation calculations (discussed in a later section), these estimated transition-state frequencies were adjusted to achieve a good fit to the experimental data. Briefly, the $(C_6H_6)_2Cr^+ \rightarrow C_6H_6Cr^+ + C_6H_6$ data were fitted by adjusting six disappearing frequencies until a best fit was obtained. For the second reaction, which has only three disappearing frequencies in TS_2, we assigned the frequency of 180 cm^{-1} to be the reaction coordinate and adjusted just the two frequencies associated with the Cr−C_6H_6 bond. All of the frequencies used in the best simulation are listed in Table 1. In this study, the quantum chemical calculations were performed using the Gaussian 98 package.[31]

Results and Discussion

1. TOF Distributions and Breakdown Diagram. TOF mass spectra of $(C_6H_6)_2Cr$ were collected in the photon energy range from 8.3 to 13.2 eV. Typical TOF distributions are shown in

TABLE 1: Frequencies Used in the Energy Distribution and RRKM Calculations

$(C_6H_6)_2Cr$[a]	34, 117, 122, 168, 260, 274, 294, 311, 360, 388, 406, 411, 432, 599, 604, 608, 612, 637, 652, 746, 766, 806, 818, 847, 848, 854, 856, 865, 931, 933, 944, 960, 963, 968, 969, 993, 993, 996, 1008, 1044, 1092, 1118, 1119, 1120, 1126, 1294, 1297, 1322, 1323, 1353, 1430, 1432, 1441, 1445, 1454, 1482, 1492, 3010, 3011, 3011, 3013, 3022, 3022, 3029, 3030, 3040, 3040, 3045, 3045
$(C_6H_6)_2Cr^+$[b]	152, 171, 171, 279, 335, 335, 409, 409, 409, 409, 415, 415, 466, 616, 616, 616, 616, 709, 709, 795, 795, 857, 857, 857, 857, 910, 910, 910, 910, 972, 972, 993, 993, 1000, 1000, 1000, 1000, 1010, 1010, 1142, 1142, 1148, 1148, 1148, 1148, 1308, 1308, 1350, 1375, 1430, 1430, 1430, 1430, 1620, 1620, 1620, 1620, 2855, 2855, 3040, 3040, 3040, 3040, 3074, 3074, 3074, 3074, 3095, 3095
TS_1[c]	16, 18, 18, 30, 35, 268, 409, 409, 409, 409, 415, 415, 466, 616, 616, 616, 616, 709, 709, 795, 795, 857, 857, 857, 857, 910, 910, 910, 910, 972, 972, 993, 993, 1000, 1000, 1000, 1000, 1010, 1010, 1142, 1142, 1148, 1148, 1148, 1148, 1308, 1308, 1350, 1375, 1430, 1430, 1430, 1430, 1620, 1620, 1620, 1620, 2855, 2855, 3040, 3040, 3040, 3040, 3074, 3074, 3074, 3074, 3095, 3095
$C_6H_6Cr^+$[d]	53, 57, 180, 408, 408, 614, 614, 671, 744, 901, 902, 995, 999, 999, 1012, 1024, 1051, 1052, 1189, 1203, 1204, 1329, 1386, 1508, 1509, 1611, 1611, 3215, 3221, 3222, 3232, 3232, 3238
TS_2[c]	−180,[e] 6, 9, 408, 408, 614, 614, 671, 744, 901, 902, 995, 999, 999, 1012, 1024, 1051, 1052, 1189, 1203, 1204, 1329, 1386, 1508, 1509, 1611, 1611, 3215, 3221, 3222, 3232, 3232, 3238

[a] Calculated at the HF level and scaled by a factor of 0.893.[30] The lowest frequency was treated as the internal rotation of benzene. [b] Reference 22. [c] Lowest six (TS_1) or two (TS_2) frequencies adjusted to fit the experimental data. [d] DFT results[23]. [e] Reaction coordinate.

Figure 2, and the experimental breakdown diagram is shown in Figure 3. In the figures, the points are the experimental data, and the solid lines are the simulation results. The ion peak at 33.3 μs is the molecular ion $(C_6H_6)_2Cr^+$ (m/z 208), whereas TOF peaks at 26.4 and 16.7 μs correspond to the product ions $C_6H_6Cr^+$ (m/z 130) and Cr^+ (m/z 52), respectively. Below 10.7 eV, the two peaks correspond to the molecular ion $(C_6H_6)_2Cr^+$ and the benzene-loss product $C_6H_6Cr^+$. At photon energies in excess of 10.7 eV, the two peaks correspond to $C_6H_6Cr^+$ and Cr^+ ions. These results, which agree with the electron ionization studies,[19−21] show that the primary fragmentation of $(C_6H_6)_2$-Cr^+ corresponds to stepwise loss of the benzene ligands. The dissociation reaction mechanism of the $(C_6H_6)_2Cr^+$ ions can be described by eq 1.

$$(C_6H_6)_2Cr^+ \xrightarrow{TS_1} C_6H_6Cr^+ + C_6H_6 \xrightarrow{TS_2} Cr^+ + 2C_6H_6 \quad (1)$$

As shown in Figure 2, the product-ion TOF distributions are asymmetric at photon energies close to the appearance energies of those product ions. This indicates that these ions are produced at various positions within the first and second acceleration regions; that is, the dissociation reaction is a slow process with lifetimes of the precursor ions in the microsecond range.

2. Simulations of the Experimental Data. Because the above experimental data were obtained at 340 K, the sample had a rather broad thermal energy distribution. At photon energies close to the dissociation limit, the product-ion TOF distributions

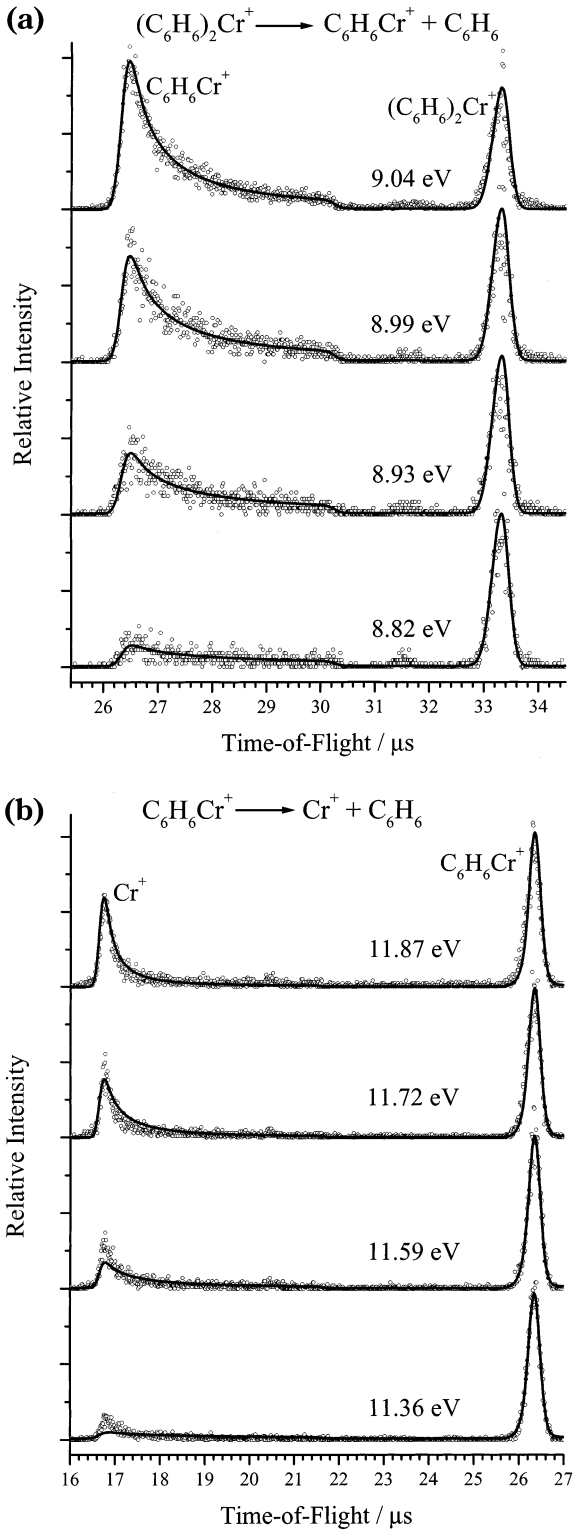

Figure 2. (a) Ion TOF distributions at selected photon energies for the first benzene-loss reaction. The points are the experimental data, and the solid lines are the simulation results. (b) Ion TOF distributions at selected photon energies for the second benzene-loss reaction.

are metastable; thus, kinetic shifts cannot be ignored. To determine accurately the appearance energies and bond energies, the experimental data must be fitted by taking into account the thermal energy distribution of the sample and the slow dissociation rate.

The statistical RRKM theory was used to calculate rate constants of the unimolecular dissociation reactions of the

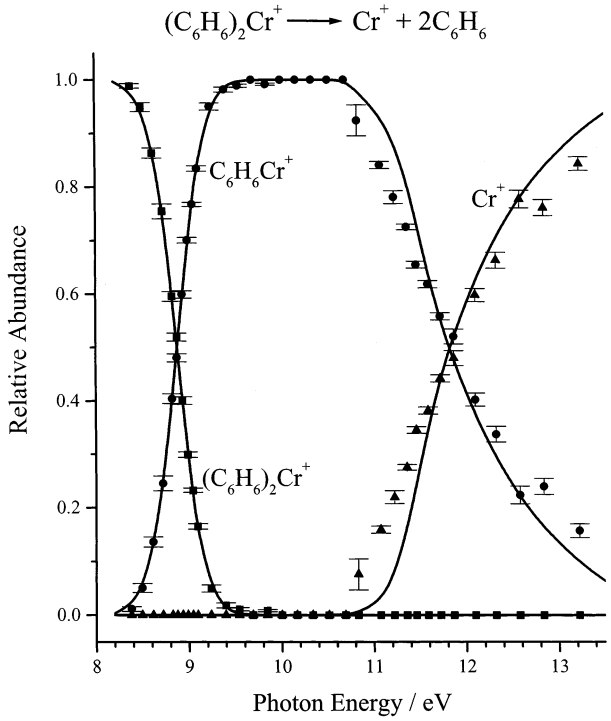

Figure 3. Breakdown diagram of $(C_6H_6)_2Cr^+$. The points are the experimental data with error estimates, and the solid lines are the simulation results.

$(C_6H_6)_2Cr^+$ ion in eq 1. The RRKM calculations were performed using the formula[27]

$$k(E) = \frac{\sigma N^{\ddagger}(E - E_0)}{h\rho(E)} \qquad (2)$$

in which σ is the symmetry parameter, E_0 is the activation energy, $N^{\ddagger}(E - E_0)$ is the sum of states of the transition state from 0 to $E - E_0$, and $\rho(E)$ is the density of states of the ion. The symmetry parameters for $(C_6H_6)_2Cr^+$ and $C_6H_6Cr^+$ used in eq 2 are 2 and 1, respectively.

The lowest vibrational frequency of $(C_6H_6)_2Cr$ is assigned as the internal rotation of the benzene ring. The energy barrier associated with the internal rotation is expected to be low for this kind of sandwich complex. Indeed, an extended Hückel calculation[2] predicts that the eclipsed conformation of $(C_6H_6)_2$-Cr is just 3.8 kJ/mol more stable than the staggered one. Thus, the lowest frequency of $(C_6H_6)_2Cr$ was treated as a rotation in the calculations of the thermal energy distribution, with the above-mentioned 3.8 kJ/mol as the estimated rotational barrier height.

To fit the experimental data, it is necessary to calculate the rate constants in terms of a thermal energy distribution. The procedure, described in detail by Sztáray and Baer,[32] involves convolutions of the thermal energy distribution of the molecule with the electron analyzer function and the rate constants. The electron analyzer function was measured from the threshold photoelectron spectra of rare gases, NO or acetylene, which have widely spaced energy levels. However, as discussed by Li et al.,[33] some adjustment of this function is necessary in certain cases. For the second dissociation step to $Cr^+ + 2C_6H_6$, the energy partitioning between C_6H_6 and $C_6H_6Cr^+$ during the first dissociation was calculated using the Klots equation.[34]

The ion TOF distributions and the breakdown diagram can be calculated using the following information: the thermal energy distribution of the precursor molecule, the acceleration electric fields, the acceleration and drift field lengths, and the adiabatic IE value of $(C_6H_6)_2Cr$. As discussed in the Introduction, several different results can be obtained from different PES measurements. An adiabatic IE value of 5.40 eV with an error of $\pm$ 0.05 eV was used in the simulation of this study. By properly adjusting the two dissociation limits, the lowest six (TS_1) or two (TS_2) vibrational frequencies of the transition states, which determine the entropies of activation and, to a limited extent, the threshold electron analyzer function; the experimental breakdown diagram; and the TOF distributions can be simultaneously fitted.

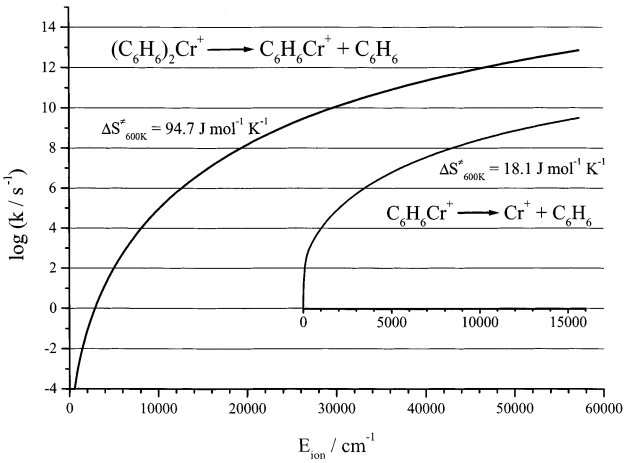

Figure 4. RRKM-calculated dissociation rate curves of $(C_6H_6)_2Cr^+$. The origin of the second dissociation rate curve is not at the dissociation limit of the second reaction; rather, it is the point that the remaining energy of the $C_6H_6Cr^+$ ion is equal to the second dissociation limit.

The simulation was carried out in a stepwise fashion. First, the breakdown diagram was modified by summing the two product ions $C_6H_6Cr^+$ and Cr^+. By simulating this breakdown diagram and the TOF distributions for the $C_6H_6Cr^+$ ion, the energy barrier height (E_1) and the transition-state frequencies for the first dissociation reaction can be determined. In the fitting for the second benzene-loss reaction, E_1 and the TS_1 frequencies determined in the first simulation were fixed, and only the energy barrier height (E_2), the TS_2 frequencies, and the threshold electron analyzer function were adjusted until the breakdown diagram and TOF distributions were simultaneously fitted.

The best fit to the experimental data was obtained with the parameters $E_1 = 2.51 \pm 0.15$ eV and $E_2 = 1.70 \pm 0.15$ eV, with the corresponding 0 K appearance energies 7.91 ± 0.15 and 9.61 ± 0.18 eV for the $C_6H_6Cr^+$ and Cr^+ ions, respectively. The simulated TOF distributions and breakdown diagram are shown in Figures 2 and 3, and the RRKM calculated rate constant curves are shown in Figure 4. We adjusted the adiabatic IE value from 5.35 to 5.45 eV and the sample temperature from 330 to 350 K and also varied the assumed internal rotational barrier of the benzene ring by multiplying it by a factor of between 50 and 200%, and we found that these adjustments made the derived appearance energies change slightly. However, any shift beyond 0.15 eV (AE_1) or 0.18 eV (AE_2) made the quality of the simulated TOF distributions and breakdown diagram become significantly worse. These tests led to the above-quoted error limits of the study.

The error limits of these appearance energies are quite large. The reason for this is the very large kinetic shift. As the rate constants in Figure 4 indicate, the dissociation limit lies about 1 eV below the energy at which the dissociation rate constant

TABLE 2: Dissociation Energy Results (in eV)

reaction	this study	other
$(C_6H_6)_2Cr+ \rightarrow C_6H_6Cr^+ + C_6H_6$	2.51 ± 0.15	2.40 ± 0.19[a]
$C_6H_6Cr^+ \rightarrow C_6H_6 + Cr^+$	1.70 ± 0.15	1.76 ± 0.10,[a] 1.62 ± 0.22,[b] 1.74 ± 0.05[c]
$(C_6H_6)_2Cr \rightarrow C_6H_6Cr + C_6H_6$	2.78 ± 0.16	
$C_6H_6Cr \rightarrow C_6H_6 + Cr$	0.06 ± 0.16	0.10 ± 0.06[c]

[a] CID results of Meyer et al.[22] [b] Theoretical result by Bauschlicher et al.[26] [c] TPEPICO results of Li et al.[23]

reaches 10^5 s^{-1}. Stated another way, the lowest data set in Figure 2a at 8.82 eV lies a full electronvolt above the true dissociation limit. Thus any errors in the slope of the $k(E)$ curves in Figure 4 will result in rather large errors in the derived onsets.

The activation entropies for the two dissociation reactions of 94.7 and 18.1 J mol^{-1} K^{-1} at 600 K are both positive, which indicates that these reactions proceed via loose transition states. This is characteristic of a simple bond-breaking reaction and permits us to associate the measured onset with a bond energy. This result is not entirely expected because the reaction $(C_6H_6)_2Cr^+(^2A_1) \rightarrow C_6H_6Cr^+(^6A_1) + C_6H_6$ takes the reactants from a doublet to a sextet potential energy surface.

Table 2 lists the dissociation energies determined in this study and the results obtained by other recent studies for comparison. Because of the previously mentioned problems with electron ionization studies, those old bond energy values are not listed in Table 2. However, the two bond energies determined by a well-controlled experiment, namely, collision-induced dissociation, in which Meyer et al.[22] modeled the onset energy with the thermal energy as well as the RRKM dissociation rate constants, yield $C_6H_6-Cr^+$ bond energies of 2.40 ± 0.19 and 1.76 ± 0.10 eV, respectively, in excellent agreement with our measurements. The $C_6H_6-Cr^+$ bond energy is also consistent with a theoretical result, 1.62 ± 0.22 eV.[26] Finally, the present results are in accord with our study on the related organometallic compound $C_6H_6Cr(CO)_3$,[23] in which the $C_6H_6-Cr^+$ bond energy was determined to be 1.74 ± 0.05 eV.

Meyer et al.[22] assumed a somewhat tighter transition state for the $C_6H_6Cr^+-C_6H_6$ bond rupture than we did. This explains, in part, their lower bond energy (2.40 eV) compared to our value of 2.51 eV. However, when we use their transition-state frequencies, the derived bond energy decreases to 2.30 eV and results in a correspondingly worse fit to our data. It appears that the two data sets are not equally sensitive to the transition-state parameters. This is perhaps consistent with the different time scales for ion detection in the TPEPICO ($\sim$10 μs) and CID ($\sim$100 μs) experiments, which requires a larger extrapolation to the onset in our data.

3. $(C_6H_6)_2Cr$ and $(C_6H_6)_2Cr^+$ Thermochemistry. Although the collision-induced dissociation and the TPEPICO data both provide ionic bond energies, the TPEPICO data contains additional information. The appearance energies connect the ionic energies to the neutral heat of formation of the $(C_6H_6)_2Cr$ molecule. Because the heats of formation of the fully dissociated products, $Cr^+ + 2C_6H_6$, are well-established, the heats of formation of $(C_6H_6)_2Cr$, $(C_6H_6)_2Cr^+$, and $C_6H_6Cr^+$ can be determined from the measured appearance energies. For instance, the 0 K heat of formation of $C_6H_6Cr^+$ is obtained using

$$\Delta_f H^o_{0\,K}(C_6H_6Cr^+) = \Delta_f H^o_{0\,K}(C_6H_6) + \Delta_f H^o_{0\,K}(Cr^+) - [AE(Cr^+) - AE(C_6H_6Cr^+)] \quad (3)$$

TABLE 3: Thermochemical Data (in kJ/mol)[a]

species	$\Delta_f H^o_{298\,K}$[b]	$\Delta_f H^o_{0\,K}$[c]	$H^o_{298\,K} - H^o_{0\,K}$[d]
$(C_6H_6)_2Cr$	286 ± 17	322 ± 17	31.06
$(C_6H_6)_2Cr^+$	804 ± 18	843 ± 18	28.62
$(C_6H_6)Cr$	475 ± 15	490 ± 15	21.11
$C_6H_6Cr^+$	968 ± 15	984 ± 15	19.90
C_6H_6	82.93 ± 0.50[e]	100.33 ± 0.50[f]	14.30
Cr	397.48 ± 4.2[g]	395.34 ± 4.2[g]	–
Cr^+	1050.28 ± 1.5[h]	1048.14 ± 1.5[g]	–

[a] In the $H^o_{298\,K} - H^o_{0\,K}$ calculations, the heat capacity of the electron was treated as 0.0 kJ/mol at all temperatures (the ion convention[36]). To convert to the electron convention, which treats the electron as a real particle, 6.197 kJ/mol should be added to the 298 K heat of formation of each ion. [b] $\Delta H^\circ_{0\,K} \rightarrow \Delta H^\circ_{298\,K}$. [c] Determined using the appearance energies determined in this study. [d] Determined using the vibrational frequencies. [e] Webbook.[37] [f] $\Delta H^\circ_{298\,K} \rightarrow \Delta H^\circ_{0\,K}$. [g] NIST–JANAF thermochemical tables.[38] [h] Converted to the ion convention, from the NIST–JANAF thermochemical tables.[38]

The interconversion between the 0 and 298 K values is performed using the following equation, for example, for neutral $(C_6H_6)_2Cr$

$$\Delta_f H^o_{298\,K}[(C_6H_6)_2Cr] = \Delta_f H^o_{0\,K}[(C_6H_6)_2Cr] - (H^o_{298\,K} - H^o_{0\,K})(\text{elements}) + [H^o_{298\,K} - H^o_{0\,K}][(C_6H_6)_2Cr] \quad (4)$$

where "elements" refers to the sum of the elements in their standard states.[35] The $(H^o_{298\,K} - H^o_{0\,K})[(C_6H_6)_2Cr]$ value is obtained from the vibrational frequencies in Table 1. Table 3 lists the 0 and 298 K heats of formation of the relevant species of this study.

The gas-phase $\Delta_f H^o_{298\,K}[(C_6H_6)_2Cr]$ obtained and listed in Table 3 is 286 ± 17 kJ/mol. A search through the literature reveals that this heat of formation is not well-established. The solid-state heat of formation of $(C_6H_6)_2Cr(s)$ has been obtained by several bomb calorimetric measurements. Among these values are 213 ± 8,[39] 220 ± 8,[40] 88 ± 33,[41] 146 ± 8,[42] and 142 ± 8 kJ/mol.[43] The most recent recommended value in a compilation by Rabinovich et al.[44] is 144 ± 4 kJ/mol. The enthalpy of sublimation based on two independent measurements of $(C_6H_6)_2Cr$ at 298 K has been reported as 78[39,40] and 91 kJ/mol.[45] Using the average of the two results and the above heats of formation of $(C_6H_6)_2Cr(s)$, the gas-phase $\Delta_f H^o_{298\,K}[(C_6H_6)_2Cr(g)]$ value has a range from 173 to 305 kJ/mol. The recommended value by Rabinovich[44] is 226 ± 4 kJ/mol, whereas the NIST Webbook[37] lists a recommended value of 234 ± 6 kJ/mol. Although our result of 286 kJ/mol clearly falls in the range of other measurements, it is considerably higher than the two most recent recommended values, but agrees extremely well with the CID value of 281 ± 20 kJ/mol reported by Meyer et al.[22] In support of our value for $\Delta_f H^o[(C_6H_6)_2Cr(g)]$, we have established the complete ionic and neutral thermochemical cycle, which is shown in Figure 5. The ion bond energies have now been reliably measured by two methods and the IE is well-established, which fixes the neutral heat of formation.

Few experimental or theoretical results have been reported for the bond energies of neutral $(C_6H_6)_2Cr$. Although the present study cannot determine the neutral bond energies directly, we can do so indirectly from the thermochemical cycle in Figure 5. If we combine the experimentally determined heat of formation of $C_6H_6Cr^+$ with the C_6H_6Cr ionization energy of 5.13 ± 0.04 eV, which was recently determined by laser ionization mass spectrometry,[46] we obtain directly the $\Delta_f H^o_{0\,K}[(C_6H_6)Cr]$ value that is listed in Table 3. As shown in Figure 5, this heat of formation, in combination with the well-known

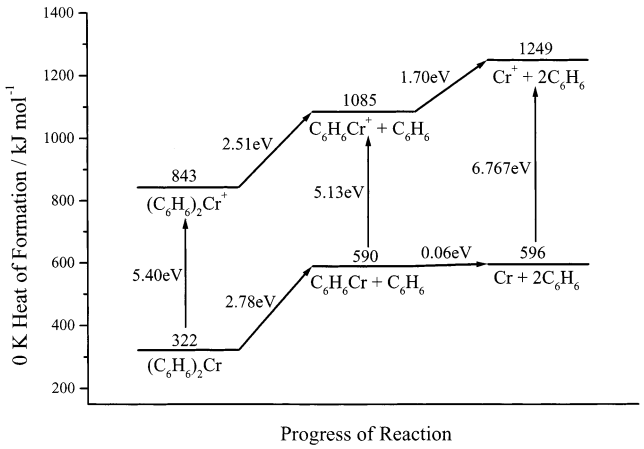

Figure 5. 0 K heat of formation diagram for the ionization and dissociation of the $(C_6H_6)_2Cr$ system.

ionization energy of the Cr atom, permits us to determine a bond energy of 0.06 eV for the neutral C_6H_6-Cr. This is within 40 meV of the bond energy determined for this molecule in our $C_6H_6Cr(CO)_3$ study. Furthermore, it agrees to within 40 meV of the value obtained by DFT calculations.[23] This very low bond energy is entirely consistent with the very large bond distance between the benzene ring and the Cr atom.

The same experimental results also lead to a $C_6H_6Cr-C_6H_6$ bond energy of 2.78 eV. No direct measurement of the neutral bond energy is available. Theoretical calculations[8] predict the sum of the two C_6H_6-Cr bond energies to be 3.76 eV (MP2) and 4.13 eV (DFT), which are higher than the results obtained in this study (2.84 eV). However, calculations on these molecules are well-known to be problematic.

In summary, we have confirmed previous measurements[22] of the ionic $Cr-C_6H_6$ bond energies and our own previous measurement[23] of the neutral $Cr-C_6H_6$ bond energy. The consistency of all of the measurements for the ionic and neutral $Cr-C_6H_6$ bond energies supports the value for the heat of formation of $(C_6H_6)_2Cr(g)$.

Conclusions

Threshold photoelectron−photoion coincidence spectroscopy has been used to investigate the dissociation kinetics of the bis-(benzene) chromium ion, $(C_6H_6)_2Cr^+$. The dissociation of the $(C_6H_6)_2Cr^+$ ion proceeds by the sequential loss of two benzene ligands. By fitting the metastable ion time-of-flight distributions and the breakdown diagram with the statistical RRKM theory, 0 K appearance energies of the two product ions were determined to be 7.91 ± 0.15 and 9.61 ± 0.18 eV, respectively. The derived ion bond energies for $C_6H_6Cr^+-C_6H_6$ and $C_6H_6-Cr^+$ are 2.51 ± 0.15 and 1.70 ± 0.15 eV, respectively. Using the known heats of formation of the fully dissociated products, benzene and Cr^+, the 298 K heats of formation of $(C_6H_6)_2Cr^+$ and $C_6H_6Cr^+$ were determined to be 804 ± 18 and 968 ± 15 kJ/mol, and the heat of formation of $(C_6H_6)_2Cr$ was found to be 286 ± 17 kJ/mol. By combining these results with the IE value of C_6H_6Cr, 5.13 ± 0.04 eV, the bond energies of neutral $(C_6H_6)Cr-C_6H_6$ and C_6H_6-Cr were determined to be 2.78 ± 0.16 and 0.06 ± 0.16 eV, respectively.

The above values are supported by the measurements of Meyer et al.,[22] who obtained ionic bond energies of 2.40 and 1.76 eV, which agree within the error limit with our results. In addition, the derived bond energy for C_6H_6Cr of 0.06 eV agrees with an independent measurement of this same bond energy in the molecule $C_6H_6Cr(CO)_3$. These results taken together provide a compelling argument to establish the 298 K heat of formation of $(C_6H_6)_2Cr$ at 286 ± 17 kJ/mol, a value that is 60 kJ/mol higher than a value recently suggested in a compilation by Rabinovich et al.[44] and 52 kJ/mol higher than the NIST Webbook value.[37]

Acknowledgment. We thank the North Carolina Supercomputer facility for a generous allotment of computer time. This work was supported by a grant from the U.S. Department of Energy, Office of Basic Energy Sciences.

References and Notes

(1) Cabelli, D. E.; Cowley, A. H.; Lagowski, J. J. *Inorg. Chim. Acta* **1982**, *57*, 195−198.
(2) Muetterties, E. L.; Bleeke, J. R.; Wucherer, E. J.; Albright, T. A. *Chem. Rev.* **1982**, *82*, 499−525.
(3) Chizhov, Y. V.; Timoshenko, M. M.; Yur′eva, L. P.; Zaitseva, N. N.; Uralets, I. A.; Kravtsov, D. N.; Asfandiarov, N. L. *J. Organomet. Chem.* **1989**, *361*, 79−87.
(4) Keulen, E.; Jellinek, F. *J. Organomet. Chem.* **1966**, *5*, 490−492.
(5) Cotton, F. A.; Dollase, W. A.; Wood, J. S. *J. Am. Chem. Soc.* **1963**, *85*, 1543−1544.
(6) Haaland, A. *Acta Chem. Scand.* **1965**, *19*, 41.
(7) Lüthi, H. P. *J. Mol. Struct. (THEOCHEM)* **1996**, *388*, 299−304.
(8) Yasuike, T.; Yabushita, S. *J. Phys. Chem. A* **1999**, *103*, 4533−4542.
(9) Williamson, R. L.; Hall, M. B. *Int. J. Quantum Chem.* **1987**, *21*, 503−512.
(10) Schleyer, P. v. R.; Kiran, B.; Simion, D. V.; Sorensen, T. S. *J. Am. Chem. Soc.* **2000**, *122*, 510−513.
(11) Bérces, A.; Ziegler, T. *J. Phys. Chem.* **1994**, *98*, 13233−13242.
(12) Evans, S.; Green, J. C.; Jackson, S. E. *J. Chem. Soc., Faraday Trans. 2* **1972**, *68*, 249−258.
(13) Brennan, J. G.; Cooper, G.; Green, J. C.; Kaltsoyannis, N.; MacDonald, M. A.; Payne, M. P.; Redfern, C. M.; Sze, K. H. *Chem. Phys.* **1992**, *164*, 271−281.
(14) Ryan, M. F.; Richardson, D. E.; Lichtenberger, D. L.; Gruhn, N. E. *Organometallics* **1994**, *13*, 1190−1199.
(15) Guest, M. F.; Hiller, I. H.; Higginson, B. R.; Lloyd, D. R. *Mol. Phys.* **1975**, *29*, 113−128.
(16) Pignataro, S.; Foffani, A.; Distefano, G. *Chem. Phys. Lett.* **1973**, *20*, 350−355.
(17) Fisanick, G. J.; Gedanken, A.; Eichelberger, T. S. I.; Kuebler, N. A.; Robin, M. B. *J. Chem. Phys.* **1981**, *75*, 5215−5225.
(18) Opitz, J.; Bruch, D.; Bünau, G. *Int. J. Mass Spectrom. Ion Processes* **1993**, *125*, 215−228.
(19) Müller, J.; Göser, P. *J. Organomet. Chem.* **1968**, *12*, 163−172.
(20) Gaivoronskii, P. E.; Larin, N. V.; Sirotkin, N. I.; Artemov, A. N.; Shushunov, N. V. *Bull. Acad. Sci. USSR, Div. Chem. Sci.* **1973**, *22*, 2557−2559.
(21) Pignataro, S.; Lossing, F. P. *J. Organomet. Chem.* **1967**, *10*, 531−534.
(22) Meyer, F.; Khan, F. A.; Armentrout, P. B. *J. Am. Chem. Soc.* **1995**, *117*, 9740−9748.
(23) Li, Y.; McGrady, J. E.; Baer, T. *J. Am. Chem. Soc.* **2002**, *124*, 4487−4494.
(24) Baer, T.; Booze, J. A.; Weitzel, K. M. Photoelectron photoion coincidence studies of ion dissociation dynamics; In *Vacuum Ultraviolet Photoionization and Photodissociation of Molecules and Clusters*; Ng, C. Y., Ed.; World Scientific: Singapore, 1991; pp 259−298.
(25) Wadt, W. R.; Hay, P. J. *J. Chem. Phys.* **1985**, *82*, 284−298.
(26) Bauschlicher, C. W., Jr.; Partridge, H.; Langhoff, S. R. *J. Phys. Chem.* **1992**, *96*, 3273−3278.
(27) Baer, T.; Hase, W. L. *Unimolecular Reaction Dynamics: Theory and Experiments*; Oxford University Press: New York, 1996.
(28) Hase, W. L. *Chem. Phys. Lett.* **1987**, *139*, 389−394.
(29) Wardlaw, D. M.; Marcus, R. A. *Adv. Chem. Phys.* **1988**, *70*, 231−263.
(30) Pople, J. A.; Scott, A. P.; Wong, M. W.; Radom, L. *Isr. J. Chem.* **1993**, *33*, 345−350.
(31) Frisch, M. J.; Trucks, G. W.; Schlegel, H. B.; Scuseria, G. E.; Robb, M. A.; Cheeseman, J. R.; Zakrzewski, V. G.; Montgomery, J. A., Jr.; Stratmann, R. E.; Burant, J. C.; Dapprich, S.; Millam, J. M.; Daniels, A. D.; Kudin, K. N.; Strain, M. C.; Farkas, O.; Tomasi, J.; Barone, V.; Cossi, M.; Cammi, R.; Mennucci, B.; Pomelli, C.; Adamo, C.; Clifford, S.; Ochterski, J.; Petersson, G. A.; Ayala, P. Y.; Cui, Q.; Morokuma, K.; Malick, D. K.; Rabuck, A. D.; Raghavachari, K.; Foresman, J. B.; Cioslowski, J.; Ortiz, J. V.; Stefanov, B. B.; Liu, G.; Liashenko, A.; Piskorz, P.; Komaromi,

I.; Gomperts, R.; Martin, R. L.; Fox, D. J.; Keith, T.; Al-Laham, M. A.; Peng, C. Y.; Nanayakkara, A.; Gonzalez, C.; Challacombe, M.; Gill, P. M. W.; Johnson, B. G.; Chen, W.; Wong, M. W.; Andres, J. L.; Head-Gordon, M.; Replogle, E. S.; Pople, J. A. *Gaussian 98*, revision A.7; Gaussian, Inc.: Pittsburgh, PA, 1998.

(32) Sztaray, B.; Baer, T. *J. Am. Chem. Soc.* **2000**, *122*, 9219−9226.

(33) Li, Y.; Sztaray, B.; Baer, T. *J. Am. Chem. Soc.* **2001**, *123*, 9388−9396.

(34) Klots, C. E. *J. Chem. Phys.* **1973**, *58*, 5364−5367.

(35) Wagman, D. D.; Evans, W. H. E.; Parker, V. B.; Schum, R. H.; Halow, I.; Mailey, S. M.; Churney, K. L.; Nuttall, R. L. *The NBS Tables of Chemical Thermodynamic Properties, J. Phys. Chem. Ref. Data Vol. 11 Suppl. 2*; NSRDS, U.S. Government Printing Office: Washington, DC, 1982.

(36) Rosenstock, H. M.; Draxl, K.; Steiner, B. W.; Herron, J. T. *J. Phys. Chem. Ref. Dat Vol. 6. Energetics of Gaseous Ions*; American Chemical Society: Washington, DC, 1977.

(37) http://webbook.nist.gov/chemistry/om/. 2000.

(38) Chase, M. W. *NIST−JANAF Thermochemical Tables*; American Institute of Physics: New York, 1998.

(39) Fischer, E. O.; Schreiner, S. *Chem. Ber.* **1958**, *91*, 2213−2215.

(40) Fischer, E. O.; Schreiner, S.; Reckziegel, A. *Chem. Ber.* **1961**, *94*, 258−262.

(41) Fischer, A. K.; Cotton, F. A.; Wilkinson, G. *J. Phys. Chem.* **1959**, *63*, 154−155.

(42) Tel'noi, V. I.; Rabinovich, I. B.; Gribov, B. G.; Pashinkin, A. S.; Salamatin, B. A.; Chernova, V. I. *Russ. J. Phys. Chem.* **1972**, *46*, 465.

(43) Connor, J. A.; Skinner, H. A.; Virmani, Y. *J. Chem. Soc., Faraday Trans.* **1973**, *69*, 1218−1225.

(44) Rabinovich, I. B.; Nistratov, V. P.; Telnoy, V. I.; Sheiman, M. S. *Thermochemical and Thermodynamic Properties of Organometallic Compounds*; Begell House, Inc.: New York, 1999.

(45) Andrews, J. T. S.; Westrum, E. F. Jr.; Bjerrum, N. *J. Organomet. Chem.* **1969**, *17*, 293−302.

(46) Kurikawa, T.; Takeda, H.; Hirano, M.; Judai, K.; Arita, T.; Nagao, S.; Nakajima, A.; Kaya, K. *Organometallics* **1999**, *18*, 1430−1438.